CHALMERS
UNIVERSITY OF TECHNOLOGY

Reliable Modeling of RF Mixers in I/Q Modulators: Experimental Validation and Parameter Extraction

Citation for the original published paper (version of record):
Hajiabdolrahim, N., Buisman, K., Wang, S. et al (2024). Reliable Modeling of RF Mixers in I/Q Modulators: Experimental Validation and Parameter
Extraction. IEEE Transactions on Communications, In Press.
http://dx.doi.org/10.1109/TCOMM.2024.3435435

(article starts on next page)

Comprehensive Modeling of RF Mixers in I/Q Modulators: Experimental Validation and Parameter Extraction

Nima Hajiabdolrahim, *Graduate Student Member, IEEE,* Koen Buisman, *Senior Member, IEEE,* Siqi Wang, and Thomas Eriksson, *Member, IEEE*

***Abstract*—This article presents an algorithm to effectively model the non-ideal behavior of RF mixers employed within the structure of I/Q modulators. The proposed model is based on the memory polynomial model, which includes nonlinearities and memory effects. To evaluate the accuracy and validity of the algorithm, a comprehensive analysis is conducted using measured data.Furthermore, this study focuses on the analysis and extraction of key parameters associated with I/Q modulators based on the proposed mixer model. Experimental comparisons are performed to assess the agreement between the measured values of each parameter and their corresponding estimated values derived from the model-based analysis. By addressing the non-ideal behavior of RF mixers and providing a methodology for parameter extraction, this research contributes to the advancement of modeling techniques for I/Q modulators. The experimental validation and comparative analysis validate the effectiveness of the proposed model in accurately capturing the intricacies of the mixers' behavior within the I/Q modulator structure.**

***Index Terms*—Mixer, I/Q Modulator, Memory Polynomial, Conversion Gain, Carrier Feed-through, IIP3, Quadrature Phase Error, I/Q Amplitude Balance.**

I. Introduction

MIXERS play a crucial role in wireless communication links as integral components of I/Q modulators and demodulators. In an ideal scenario, mixers within an I/Q modulator should operate independently, solely multiplying the intermediate frequency (IF) input signals with the local oscillator (LO) signal to produce the desired radio frequency (RF) output signal. However, in practical applications, non-ideal behaviors can manifest as a result of various factors such as nonlinearities, memory effects, and leakages between different ports of the I/Q modulator [1]–[4]. To accurately predict and account for these non-ideal behaviors, it is necessary to develop a mixer model that incorporates two input ports and one output port. This model serves as a valuable tool for understanding and characterizing the performance deviations exhibited by mixers within I/Q modulators. By considering the interplay between the input signals and the LO signal, the mixer model enables the analysis and quantification of key factors that contribute to the overall system performance. Nonlinearities in mixers can arise in the form of phenomena such as device saturation and cross-modulation effects, which introduce undesired signal distortion and impair the fidelity of the output RF signal. Memory effects, on the other hand, encompass phenomena where the mixer's output depends not only on the instantaneous input signals but also on past signals and their interactions. These effects can manifest as unwanted memory in the system, leading to signal distortions and compromising the accuracy of data transmission. Moreover, leakages between different ports of the I/Q modulator can occur, resulting in unwanted coupling between the I/Q channels. These leakages can lead to impairments such as quadrature amplitude and phase imbalances, and carrier feed-through. Understanding and modeling these non-ideal behaviors are essential for optimizing the performance of I/Q modulators and ensuring the robustness of wireless communication systems. By developing a comprehensive mixer model that captures these non-ideal behaviors, researchers and engineers can gain deeper insights into the intricacies of I/Q modulators.

Various methodologies have been proposed for modeling mixers, with two primary approaches being the circuit-level modeling approach [1], [5], and the behavioral modeling approaches [6]–[8]. In [9], two distinct approaches are presented for modeling the nonlinearities in a mixer, involving the consideration of nonlinearities either before or after an ideal mixing block. However, the non-ideal effects from the LO signal, including LO leakage and additional non-linearities, are not addressed. One of the most comprehensive models that have been proposed for mixers is presented in [7], where a multi-box model has been proposed for modeling the memory effects and the nonlinearities of a mixer separately, however, the non-ideal effects generated by the LO signal has not been explored. From another point of view, many studies have been made on modeling the non-ideal behavior of I/Q modulators, where the main source of non-linearity is the mixers that are implemented in in-phase and quadrature branches. For example, in [10] and [11] non-ideal behavior of an I/Q modulator is modeled as a frequency-selective I/Q mismatch model, which can model the memory effects of an I/Q modulator and the linear leakages that can exist between in-phase and

Nima Hajiabdolrahim and Thomas Eriksson are with the Department of Electrical Engineering, Chalmers University of Technology, SE-412 96 Gothenburg, Sweden (email: nimahaj@chalmers.se; thomase@chalmers.se).

Koen Buisman is with the Department of Microtechnology and Nanoscience, Chalmers University of Technology, SE-412 96 Gothenburg, Sweden, and also with the Department of Electrical and Electronic Engineering, University of Surrey, Surrey GU2 7XH, U.K (email: k.buisman@chalmers.se; k.buisman@surrey.ac.uk).

Siqi Wang was with the Department of Electrical Engineering, Chalmers University of Technology, SE-412 96 Gothenburg, Sweden. He is now with the Laboratoire de Génie Electrique et Electronique de Paris, CNRS, Sorbonne Université, 75252 Paris, France (email: : siqiw@chalmers.se; siqi.wang@sorbonne-universite.fr).

quadrature branches, however, it does not consider the higher order nonlinear effects from the input signal and the possible leakages from LO port to the output port. In [12] a Volterra model has been proposed for modeling the non-linearities and the memory effects of I/Q modulators, but again the non-ideal effects imposed by the LO signal are neglected.

When modeling mixers, it is crucial to consider whether they should be analyzed independently or as integral components of I/Q modulators or demodulators. For instance, in the models developed in [6]–[8], mixers are studied independently, however in the I/Q modulator structure, there would be some additional leakages between the mixers implemented in in-phase and quadrature branches [10], [12]. On the other hand, if I/Q modulators are modeled autonomously, without applying the implemented mixers' models, some possible crosstalk nonlinear terms and some possible leaks from LO signal are neglected, which plays a key role in mixer modeling [13], [14]. Hence, it is evident that the development of a new model specifically tailored for RF mixers, considering their unique utilization within an I/Q modulator structure, would yield significant benefits. Therefore, in this paper, we propose such a composite model.

In the realm of wireless transceiver design, careful consideration must be given to the crucial characteristics of I/Q modulators [15]–[17]. Consequently, leveraging a developed mixer model enables the extraction of essential parameters specific to I/Q modulators. This approach provides a practical means to accurately determine the crucial parameters that govern the behavior and performance of I/Q modulators.

This study presents a comprehensive model specifically designed for mixers operating within an I/Q modulator configuration. The proposed model demonstrates its capability to accurately predict the non-ideal behavior exhibited by mixers. To assess the effectiveness of the model, a series of experimental measurements were conducted using a laboratory setup. Consequently, the main contributions of this work can be summarized as follows:

- Development of a model based on memory polynomials that effectively captures the non-ideal behavior of mixers employed in I/Q modulators. The model offers acceptable precision in predicting the performance deviations of the mixers.
- Validation of the proposed model through meticulous measurement experiments. The experimental results provide empirical evidence of the model's accuracy and reliability.
- Analysis and extraction of key parameters associated with I/Q modulators based on the proposed model. This analysis offers valuable insights into the underlying characteristics and performance metrics of I/Q modulators.

These contributions collectively enhance our understanding and modeling capabilities of mixers operating within an I/Q modulator configuration. The proposed model provides a valuable tool for system-level design, optimization, and performance evaluation of wireless transceivers.

The paper is structured as follows; Section II presents the proposed model in two steps. First, the proposed structure is outlined, followed by the introduction of the mathematical model based on memory polynomials. Section III describes the development of a measurement setup used to validate the proposed model, and the corresponding measurement results are reported. In Section IV, key parameters of I/Q modulators are discussed, along with the procedure for extracting these parameters. Finally, Section V concludes the paper by providing a brief discussion of the results obtained from this research work.

II. Proposed Algorithm

The primary objective of this research is to develop a comprehensive model for mixers that can effectively predict their non-ideal behaviors. Since mixers are principally implemented as a part of I/Q modulators and demodulators in communication links, the proposed model is introduced in an I/Q modulator structure. In the following subsections, first, the proposed structure for I/Q modulators is introduced, then the proposed mathematical model for mixers is discussed.

A. Proposed Structure

I/Q modulators consist of two mixers, one in the in-phase branch and one in the quadrature branch. In the ideal case, there would be no correlation between the two mixers inside an I/Q modulator and each mixer only multiplies its IF input with the LO signal to generate the target RF signal at its output port. Nevertheless, in many applications, there are leakages between in-phase and quadrature branches inside an I/Q modulator and in each branch the mixer output depends on both IF input signals in in-phase and quadrature branches. Thus, in order to track the non-ideal behavior of mixers implemented in an I/Q modulator, each mixer should be considered as a component with two IF inputs plus an LO input.

Mixer's input and output signals are basically in different frequency bands. For example, in the I/Q modulator case, each mixer has a data input signal in IF band, an LO input signal in RF band, and an RF output signal which is equal to the multiplication of the two input signals and is in the same frequency band as the LO signal. According to the fact that input and output signals are in different frequency bands, modeling the non-ideal behaviour of a mixer based on its pure input and output signals is a challenging task and from signal processing point of view it is more preferable to have all the input and output signals in the same frequency band [18]. On the other hand, based on the study carried out in [19], it can be concluded that the mixer's behaviour can be observed by considering the baseband equivalent signals of the RF input and output signals, or in other words it can be stated that we can construct our mixer model based on the baseband equivalent signals rather than RF signals without any loss of generality.

Correspondingly, the structure that we use for modeling mixers as a part of I/Q modulators is illustrated in Fig.1, which is based on baseband equivalent signals.

In Figure 1, $x[n]$, $s[n]$ and $y[n]$ are all baseband signals, where $x_r[n]$ and $x_i[n]$ are real and imaginary parts of $x[n]$, and $s_r[n]$ and $s_i[n]$ are real and imaginary parts of $s[n]$, respectively. $\mathbf{F}_I$ and $\mathbf{F}_Q$ are the main components of the

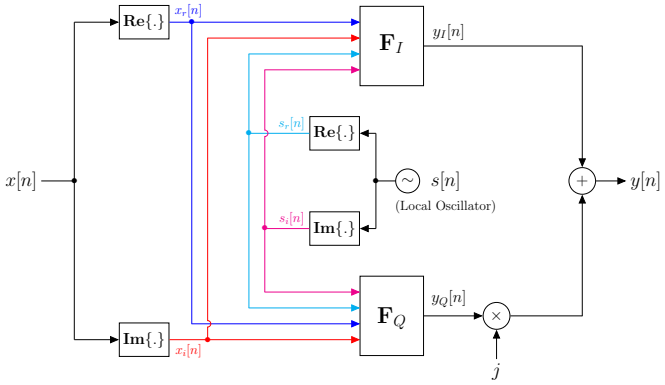

Fig. 1. Proposed structure for modeling mixers as elements of I/Q modulators.

proposed structure which are supposed to model the non-ideal behavior of the mixers implemented in the in-phase branch and quadrature branch, respectively.

B. Proposed Model

There are different ways to model a non-linear dynamic function, where, based on [20], [21] it can be stated that any time-invariant, non-linear dynamic function has an expression in the form of Volterra series. Therefore, one reasonable option for modeling $\mathbf{F}_I$ and $\mathbf{F}_Q$ blocks might be applying a Volterra series structure to be able to track any non-ideal behavior of the mixers. However, as discussed in [22], a memory polynomial structure can achieve similar accuracy level in estimating the non-ideal behavior of a mixer with lower complexity. Thus, in this work, a memory polynomial structure with real-valued inputs is employed at $\mathbf{F}_I$ and $\mathbf{F}_Q$ blocks, and their output signals can be expressed as follows [23]

$$\begin{aligned} y_I[n] &= F_I\left(x_r[n], x_i[n], s_r[n], s_i[n]\right) \\ &= \sum_{m=0}^{M_I} \sum_{p_1=0}^{P^r_{x,I}} \sum_{p_2=0}^{P^i_{x,I}} \sum_{p_3=0}^{P^r_{s,I}} \sum_{p_4=0}^{P^i_{s,I}} a\left(m, p_1, p_2, p_3, p_4\right) \times \\ &\qquad \Big(x_r^{p_1}[n-m] x_i^{p_2}[n-m] s_r^{p_3}[n-m] s_i^{p_4}[n-m]\Big), \end{aligned} \tag{1}$$

$$\begin{aligned} y_Q[n] &= F_Q\left(x_r[n], x_i[n], s_r[n], s_i[n]\right) \\ &= \sum_{m=0}^{M_Q} \sum_{p_1=0}^{P^r_{x,Q}} \sum_{p_2=0}^{P^i_{x,Q}} \sum_{p_3=0}^{P^r_{s,Q}} \sum_{p_4=0}^{P^i_{s,Q}} b\left(m, p_1, p_2, p_3, p_4\right) \times \\ &\qquad \Big(x_r^{p_1}[n-m] x_i^{p_2}[n-m] s_r^{p_3}[n-m] s_i^{p_4}[n-m]\Big). \end{aligned} \tag{2}$$

In (1) and (2), $x_r[n]$, $x_i[n]$, $s_r[n]$ and $s_i[n]$ are real and imaginary parts of the data input signal and the LO input signal to the mixers, respectively. In (1) and (2), different non-linearity orders have been assumed for different inputs in different branches; $P^r_{x,I}$, $P^i_{x,I}$, $P^r_{s,I}$ and $P^i_{s,I}$ are the non-linearity orders of $x_r[n]$, $x_i[n]$, $s_r[n]$ and $s_i[n]$ in the in-phase branch, respectively, while $P^r_{x,Q}$, $P^i_{x,Q}$, $P^r_{s,Q}$ and $P^i_{s,Q}$ are the non-linearity orders of the input signals in the same order in quadrature branch. Moreover, M_I and M_Q are the memory depths in in-phase and quadrature branched in equations (1) and (2). Finally, a and b are the coefficients of applied memory polynomials for modeling F_I and F_Q blocks, which are the 2 mixers in different branches of the considered I/Q modulator structure in Fig. 1.

For each set of (m, p_1, p_2, p_3, p_4), the term $x_r^{p_1}[n-m] x_i^{p_2}[n-m] s_r^{p_3}[n-m] s_i^{p_4}[n-m]$ constructs a basis function for the memory polynomial expressions in (1) and (2). If the k-th basis function is represented by $\Phi_k[n]$, then equations (1) and (2) can be re-expressed as follows

$$y_I[n] = \sum_{k=1}^{K_I} \alpha_k \Phi_k[n], \tag{3a}$$

$$y_Q[n] = \sum_{k=1}^{K_Q} \beta_k \Phi_k[n], \tag{3b}$$

where K_I and K_Q are the number of different combinations of valid values of memories and non-linearity orders that satisfy the constraints in (1) and (2), for in-phase and quadrature branches, respectively. Additionally, α_k and β_k are the coefficients of k-th basis function in in-phase and quadrature branches. In general, the number of basis functions is different in in-phase and quadrature branches, this means that there might be some basis functions in (3a) that does not appear in (3b), and vice versa. If the non-linearity orders of different inputs and memory depths are identical in both the in-phase and quadrature branches, then all the basis functions utilized in (3a) would also be present in (3b).

For simplicity in notation, the proposed model for mixers is referred to as 4-dimensional memory polynomial (4D-MP) model in the remaining of this article.

III. Measurement

In this section, the validity of the proposed 4D-MP model for mixers is examined through experiments over the measurement setup illustrated in Figure 2. The main parts of this setup are the transmitter part, the modulator part, the LO part, and the receiver part. In the transmitter part, the digital input signal, $x[n]$, is separated into in-phase and quadrature inputs first, then the continuous time input signals are constructed using Active Technologies AT-1212 DAC which creates 1.25 Giga samples per second. In the LO part, first, the digitally generated LO signal is converted to an analog LO signal by using a second DAC used at the transmitter, then in order to be able to measure the LO signal, a directional coupler is used to couple a small fraction the LO signal that is measured by implementing a low-pass filter (LPF) with a cut-off frequency of 720 MHz and an analog to digital converter (ADC). The ADC that is used in the developed setup in Figure 2 is an NI 5771 from National Instruments with a sampling rate of 1.5 Giga samples per second. The other output of the coupler is imported to the I/Q modulator part. In the modulator part, an ADL5385 from Analog Devices is used as an I/Q modulator, where the analog signals generated at the transmitter part are imported as the in-phase and quadrature inputs and the analog LO signal is also fed as the LO input. In addition, there is a frequency

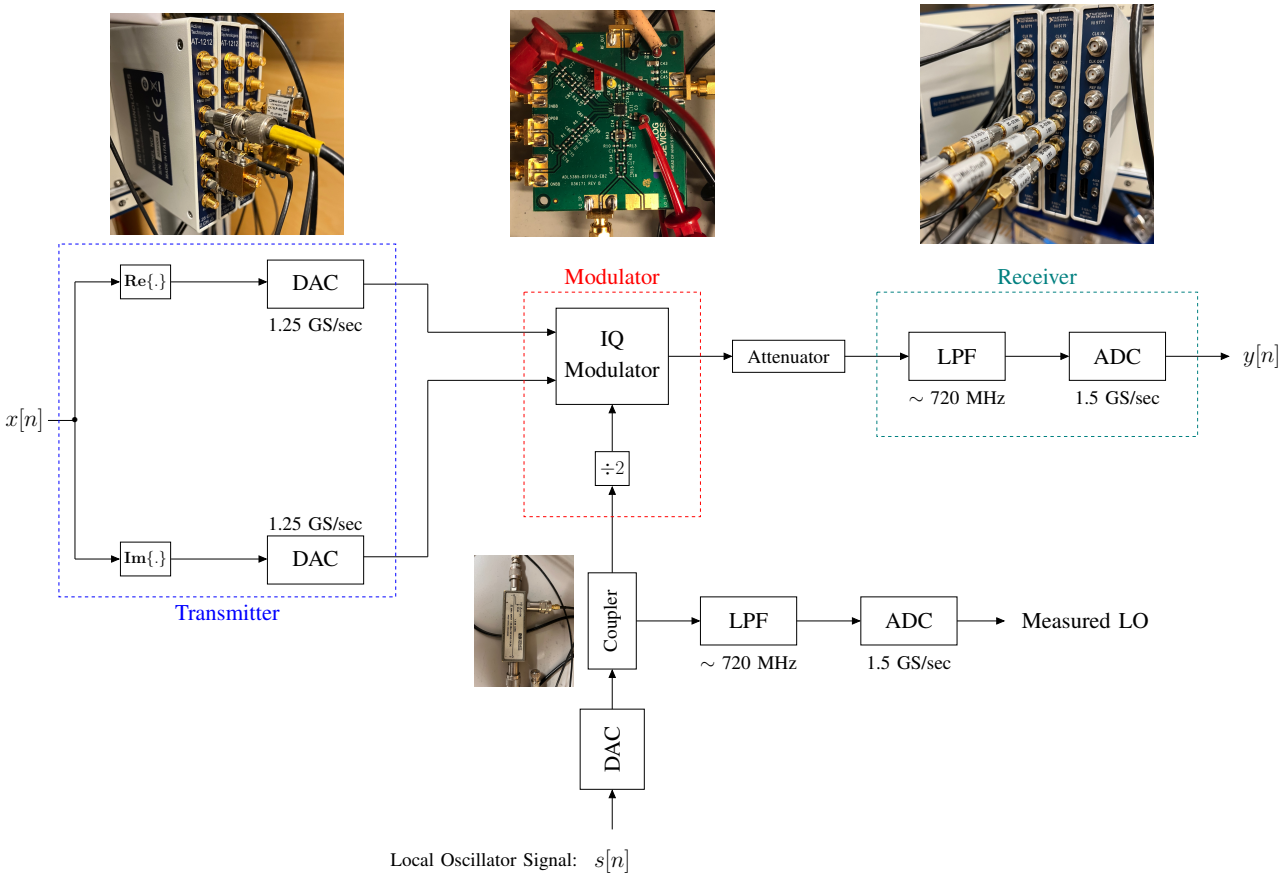

Fig. 2. Measurement setup developed for validating the proposed 4D-MP model for mixers.

divider inside the modulator, which divides the frequency of the LO signal by a factor of 2, so the imported LO signal to the modulator should be centered at twice the intended carrier frequency. The main reason for implementing this frequency divider is to facilitate the 90 degrees LO generation inside the I/Q modulator. In the receiver part, the RF signal is first passed through an LPF and then fed into an ADC to get a digital measurement of the RF output of the I/Q modulator, which can be used for developing and validating the proposed 4D-MP model. The RF output of the I/Q modulator is passed through an attenuator before being measured at the receiver part. The main reason for using an attenuator is to guarantee that the measured distortion at the output signal is dominated by the distortion generated by the I/Q modulator under test, otherwise, there is a risk of introducing additional distortion from the ADC at the receiver part.

In order to uniquely specify the utilized I/Q modulator based on the developed 4D-MP model, it is required to estimate the model's parameters based on a set of training data. Therefore, a sequence of 4.2×10^6 root raised cosine pulse-shaped 64-QAM samples with a baseband bandwidth of 47 MHz is imported as $x[n]$ to the measurement setup given in Figure 2. In order to compensate for the difference between the sampling rates of the DACs and the ADCs, $x[n]$ needs to be resampled with ratio $\frac{5}{6}$ before being fed to the measurement setup. The LO signal, $s[n]$, is a perfect cosine function centered at frequency $f_{\text{LO}} = 500$ MHz, however, due to the frequency division inside the modulator block the effective carrier frequency would be $f_c = 250$ MHz. In order to be able to observe the possible nonlinear effects of LO signal at the output signal it would be necessary to have variations in the magnitude and phase of the lowpass equivalent signal of the LO signal, so in order to create these variations in LO signal the training sequence is split into subsequences of length 1.5×10^5 samples, where for different subsequences the magnitude and phase of the LO signal is different. The spectrum of an example input signal and the corresponding output signal of the measurement setup are depicted in Figure 3, where the input signal and the LO signal are generated in the way described above. Additionally, the power and the initial phase of the applied LO signal are fixed. As mentioned in Figure 3, there is visible spectral regrowth in the spectrum of the output signal of the measurement setup which indicates the existence of some nonlinearities at the I/Q modulator. Furthermore, Figure 3 displays noticeable harmonic distortions across various frequency bands, highlighting the significance of implementing a suitable band-pass filter to prevent interference in adjacent frequency ranges.

By following the same procedure as described in [22], it is possible to fit the proposed 4D-MP model to the measured I/Q

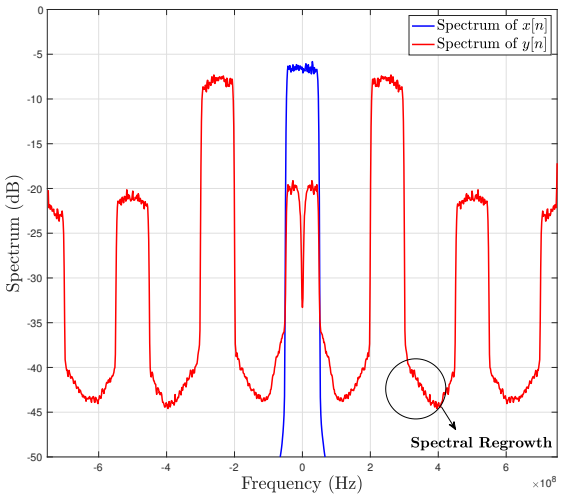

Fig. 3. Spectrum of an example input signal to the measurement setup and the corresponding output signal.

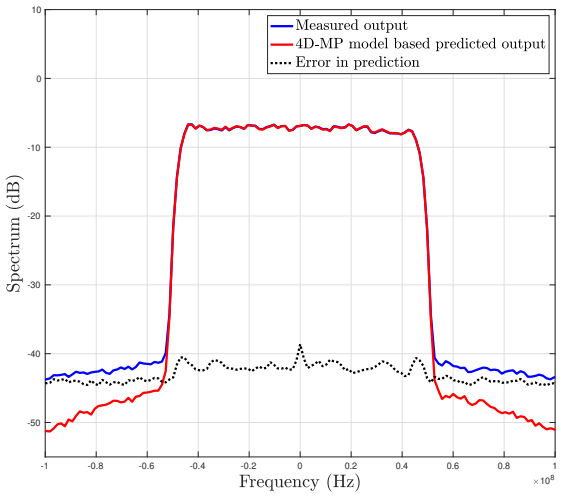

Fig. 4. Spectrum of the measured output signal (solid blue line), the simulated output signal to the same input sequence (solid red line) and the error signal which is the difference between the measured output and the predicted output signals (dotted line).

modulator based on a set of training data. The parameters of the 4D-MP model that are required for modeling the specific I/Q modulator measured in Figure 2 are given in Table I. It should be noted that a separate sequence of data is used for evaluating the model and finding the set of parameters that minimizes the normalized mean squared error (NMSE).

As mentioned in Table I, the maximum nonlinearity order that can be observed at the output of the measured I/Q modulator is the 5th order nonlinearity, however, the contribution of LO signal's real and imaginary parts, $s_r[n]$ and $s_i[n]$, to these nonlinearities is only in the form of 1st order terms, which means that the effects of LO signal at the output can be formulated in term of linear leakages or it can appear as terms with the form of $x_r^{p_1}[n-l]x_i^{p_2}[n-l]s_r[n-l]$ or $x_r^{p_1}[n-l]x_i^{p_2}[n-l]s_i[n-l]$. Moreover, there is a non-negligible amount of memory in the output of the measured I/Q modulator, which makes the output signal's samples dependent on up to 10 previous samples.

By extracting the coefficients of the 4D-MP model for the mixers in the in-phase and quadrature branches, it becomes feasible to develop an I/Q modulator simulator. This allows for expressing the outputs of the in-phase and quadrature branches, given an arbitrary set of input signal and LO signal, using the basis functions and the extracted coefficients, as illustrated in equations (3). The spectrum of the measured output signal and the simulated output signal to the same sequence of 64-QAM pulse-shaped samples with 47 MHz bandwidth are depicted in Figure 4. The spectrums plotted in Figure. 4 belong to the lowpass equivalents of the measured and the simulated output signals, so they are centered around zero.

Figure 4 clearly demonstrates that the spectrum of the prediction error signal (indicated by the black dotted line) closely aligns with the noise floor level of the measurement setup. This confirms that, within the measured frequency band, the I/Q modulator simulator developed using the 4D-MP model can accurately predict the actual output signal of the measured I/Q modulator with high precision. However, for different frequency bands the parameters of the 4D-MP model might be different, so for a certain frequency band a specific simulator needs to be developed to predict the behavior of the I/Q modulator.

TABLE I
PARAMETERS SET FOR ADAPTING THE 4D-MP MODEL TO THE MEASURED DATA SET.

Parameter	Value
Length of training sequence	4200000 samples
Length of evaluating sequence	1350000 samples
Memory depth	10 samples (6.7 ns)
Non-linearity order of $s[n]$	1
Non-linearity order of $x_r[n]$ (= $\max\{P^r_{x,I}, P^r_{x,Q}\}$)	5
Non-linearity order of $x_i[n]$ (= $\max\{P^i_{x,I}, P^i_{x,Q}\}$)	5
Number of coefficients	2×561
NMSE	-30.98 dB

IV. I/Q MODULATOR'S KEY PARAMETERS

There are several essential parameters that characterize the behavior of I/Q modulators and are typically documented in datasheets. These parameters play a significant role in hardware system design. While they can be measured separately under specific conditions, it is possible to extract these parameters directly from the proposed 4D-MP model for mixers. Some of the key parameters of I/Q modulators include

- Conversion gain,
- Carrier feed-through,

- Third-order intermodulation intercept point (IIP3),
- Quadrature phase error, and
- I/Q amplitude balance.

Each of these parameters will be discussed individually in the following subsections.

A. Conversion Gain

Conversion gain which is defined as the up-converting gain or down-converting gain of a mixer, can be expressed as the ratio between the magnitude of the desired output signal and the magnitude of the input signal. If it can be assumed that the conversion gain is constant over all the desired frequency band, one can express the conversion gain by $\sqrt{\frac{P_{\text{out}}}{P_{\text{in}}}}$, where P_{out} is the power of desired output signal and P_{in} is the power of input data signal. The desired output signal of a mixer is a part of the mixer output signal that is located in the desired frequency band, which is usually extracted by applying an appropriate filter.

In the general case, in order to calculate the conversion gain according to the proposed 4D-MP model, it is required to first extract the part of the output signal that is located in desired frequency band. As discussed in [24], based on extended Bussgang decomposition for non-linear systems with memory, the I and Q outputs of an I/Q modulator can be expressed as

$$y_I[n] = h_{II}[n] * x_I[n] + h_{IQ}[n] * x_Q[n] + d_I[n], \tag{4a}$$
$$y_Q[n] = h_{QI}[n] * x_I[n] + h_{QQ}[n] * x_Q[n] + d_Q[n], \tag{4b}$$

where $x_I[n] = \mathcal{R}e\{x[n]\}$ and $x_Q[n] = \mathcal{I}m\{x[n]\}$ are in-phase and quadrature inputs to the I/Q modulator, and $d_I[n]$ and $d_Q[n]$ are the remaining uncorrelated distortion terms in I and Q branches respectively, which means that both $d_I[n]$ and $d_Q[n]$ are uncorrelated with $x_I[n]$ and $x_Q[n]$. In addition, $h_{II}[n]$, $h_{IQ}[n]$, $h_{QI}[n]$ and $h_{QQ}[n]$ are linear causal filters in (4). In equations of (4) there is no Gaussian assumption on the input signals, $x_I[n]$ and $x_Q[n]$, however as discussed in [25], [26], it is always possible to decompose the output of a non-linear system as a linear combination of the input signal and an uncorrelated distortion term. Moreover, as discussed in [27], it is more common to introduce distinct conversion gains for in-phase and quadrature branches of an I/Q modulator. Therefore, in order to find the conversion gain for the in-phase branch, the quadrature input should be terminated. By doing that, the equations in (4) need to be modified as

$$y_I[n] = h_{II}[n] * x_I[n] + d_I[n], \tag{5a}$$
$$y_Q[n] = h_{QI}[n] * x_I[n] + d_Q[n]. \tag{5b}$$

The baseband equivalent of the I/Q modulator output signal would be equal to

$$y[n] = y_I[n] + jy_Q[n] = h_I[n] * x_I[n] + d[n], \tag{6}$$

where $h_I[n] = h_{II}[n] + jh_{QI}[n]$ and $d[n] = d_I[n] + jd_Q[n]$. So the conversion gain frequency response for the in-phase branch would be equal to the frequency response of $h_I[n]$. Thus, finding the conversion gain frequency response for in-phase branch would be equivalent to finding the Fourier transform of $h_I[n] = h_{II}[n] + jh_{QI}[n]$.

At the first step of finding $h_I[n]$, it can be stated that $y_I[n]$ and $y_Q[n]$ will depend on $x_I[n-l]$ only for $l = 0, 1, \cdots, M$, since in the developed 4D-MP model the maximum memory of the system is assumed as M. Therefore, equations in (5) can be written as

$$y_I[n] = \sum_{l=0}^{M} h_{II}[l] x_I[n-l] + d_I[n], \tag{7a}$$
$$y_Q[n] = \sum_{l=0}^{M} h_{QI}[l] x_I[n-l] + d_Q[n]. \tag{7b}$$

In the next step, by formulating the cross correlation functions between $y_I[n]$ or $y_Q[n]$, and $x_I[n-k]$ for $k = 0, 1, \cdots, M$, the following equations can be concluded

$$R_{y_I x_I}[k] = \sum_{l=0}^{M} h_{II}[l] R_{x_I x_I}[k-l] \quad , \; k = 0, 1, \cdots, M, \tag{8a}$$

$$R_{y_Q x_I}[k] = \sum_{l=0}^{M} h_{QI}[l] R_{x_I x_I}[k-l] \quad , \; k = 0, 1, \cdots, M. \tag{8b}$$

Now, by using the definition of basis functions given in (3), $R_{y_I x_I}$, $R_{y_Q x_I}$ and $R_{x_I x_I}$ can be calculated as

$$\begin{aligned} R_{y_I x_I}[k] &= \mathbb{E}\{y_I[n] x_I[n-k]\} \\ &= \sum_{m=1}^{K_I} \alpha_m \mathbb{E}\{\Phi_m[n] x_I[n-k]\}, \end{aligned} \tag{9a}$$

$$\begin{aligned} R_{y_Q x_I}[k] &= \mathbb{E}\{y_Q[n] x_I[n-k]\} \\ &= \sum_{m=1}^{K_Q} \beta_m \mathbb{E}\{\Phi_m[n] x_I[n-k]\}, \end{aligned} \tag{9b}$$

$$R_{x_I x_I}[k] = \mathbb{E}\{x_I[n] x_I[n-k]\}. \tag{9c}$$

Furthermore, since $d_I[n]$ and $d_Q[n]$ are uncorrelated with $x_I[n]$, their cross correlation functions with different delayed versions of $x_I[n]$ are assumed equal to 0 in (8) [24]. In the next step, the set of linear equations in (8) can be rewritten in the following vector forms

$$\mathbf{R}_{y_I x_I} = \mathbf{\Lambda}_{x_I} \mathbf{h}_{II}, \tag{10a}$$
$$\mathbf{R}_{y_Q x_I} = \mathbf{\Lambda}_{x_I} \mathbf{h}_{QI}, \tag{10b}$$

where $\mathbf{R}_{y_I x_I}$, $\mathbf{R}_{y_Q x_I}$, $\mathbf{h}_{II}$ and $\mathbf{h}_{QI}$ are $(M+1) \times 1$ vectors defined as follows

$$\mathbf{R}_{y_I x_I} = [R_{y_I x_I}[0] \quad R_{y_I x_I}[1] \quad \cdots \quad R_{y_I x_I}[M]]^T, \tag{11a}$$
$$\mathbf{R}_{y_Q x_I} = [R_{y_Q x_I}[0] \quad R_{y_Q x_I}[1] \quad \cdots \quad R_{y_Q x_I}[M]]^T, \tag{11b}$$
$$\mathbf{h}_{II} = [h_{II}[0] \quad h_{II}[1] \quad \cdots \quad h_{II}[M]]^T, \tag{11c}$$
$$\mathbf{h}_{QI} = [h_{QI}[0] \quad h_{QI}[1] \quad \cdots \quad h_{QI}[M]]^T, \tag{11d}$$

and $\mathbf{\Lambda}_{x_I}$ is an $(M+1) \times (M+1)$ matrix, whose elements are $\Lambda_{x_I}(i,j) = R_{x_I x_I}[i-j]$ for $i = 1, 2, \cdots, M+1$ and

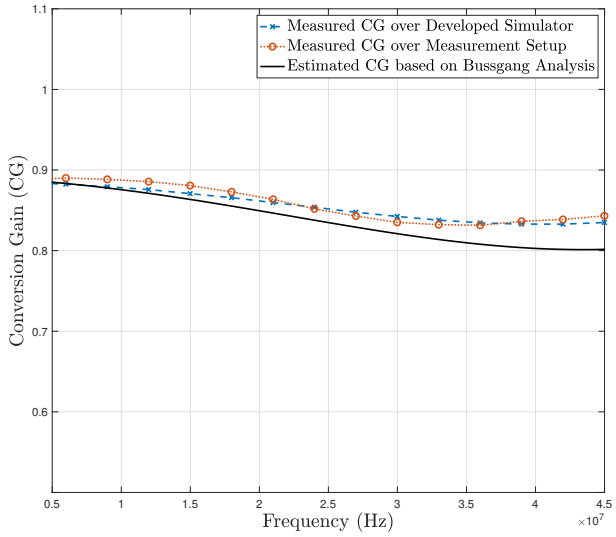

Fig. 5. Predicted and measured conversion gain frequency response.

$j = 1, 2, \cdots, M+1$. Next, by solving equations in (10) for $\mathbf{h}_{II}$ and $\mathbf{h}_{QI}$, it can be stated that

$$\mathbf{h}_{II} = \mathbf{\Lambda}_{x_I}^{-1}\mathbf{R}_{y_I x_I}, \tag{12a}$$

$$\mathbf{h}_{QI} = \mathbf{\Lambda}_{x_I}^{-1}\mathbf{R}_{y_Q x_I}. \tag{12b}$$

Finally, once $\mathbf{h}_{II}$ and $\mathbf{h}_{QI}$ are specified, the conversion gain frequency response can be smoothly found by calculating the FFT of $\mathbf{h}_I = \mathbf{h}_{II} + j\mathbf{h}_{QI}$. For instance, the predicted conversion gain frequency response of the measured I/Q modulator is depicted in Figure 5 versus the measured value of conversion gain at different frequencies. The data signal that is used for developing the 4D-MP model has a baseband bandwidth of 47 MHz, so the conversion gain can be predicted only in the same frequency band. In Figure 5 the dashed blue line represents the conversion gain that is measured by applying a multi-tone signal to an I/Q modulator modeled by the proposed 4D-MP model, the dotted red line represents the conversion gain that is measured by transmitting a multi-tone signal over the measurement setup expressed in Figure 2, and the solid black line represents the predicted conversion gain based on Bussgang expression analysis. As illustrated in Figure 5, the measured conversion gain based on 4D-MP model follows the conversion gain measured in practice, however, there is less than 2 percent difference between these 2 measured conversion gains. The measured conversion gain shows a slight deviation from the predicted conversion gain obtained through Bussgang analysis, primarily attributed to the utilization of different input signals. As described in [27], a real sinusoidal waveform was employed as the input signal for measuring the conversion gain of the I/Q modulator at various frequencies. Conversely, for deriving the predicted conversion gain, a wideband QAM modulated signal was employed to estimate the $\mathbf{h}_{II}$ and $\mathbf{h}_{QI}$ filters across the measured frequency band. Consequently, the input signals exhibit distinct structures, leading to variations in conversion gains. When a wideband input signal is employed, the presence of more nonlinearities in the system becomes evident, as the second and higher-order terms in the I/Q modulator model generate in-band distortion. However, when a single tone input signal is employed, no in-band distortion arises from the nonlinear terms. Therefore, it is expected that the predicted conversion gain will deviate from the measured conversion gain. Furthermore, as depicted in 5, it has been experimentally validated that the slight discrepancy in the conversion gain plots is primarily caused by the introduction of additional in-band distortion when utilizing a wideband input signal compared with the measured conversion gain for single tone input signal. In conclusion, it can be inferred that the predicted conversion gain, derived from the wideband signal transmission, aligns more closely with the practical conversion gain observed in actual communication links, as it accurately accounts for the presence of in-band distortion.

B. Carrier Feed-through

Carrier feed-through is defined as a parameter for measuring the leakages from the LO port to the mixer's output port. In order to measure the carrier feed-through it is beneficial to use the Bussgang decomposition technique for memory polynomials to separate the leaked LO signal term from other parts of the output signal. Therefore, based on the same approach as in (4) the I and Q outputs can be expressed in the following form

$$y_I[n] = g_{II}[n] * s_I[n] + g_{IQ}[n] * s_Q[n] + \tilde{d}_I[n], \tag{13a}$$

$$y_Q[n] = g_{QI}[n] * s_I[n] + g_{QQ}[n] * s_Q[n] + \tilde{d}_Q[n], \tag{13b}$$

where $s_I[n] = \mathcal{R}e\{s[n]\}$ and $s_Q[n] = \mathcal{I}m\{s[n]\}$ are the real and imaginary parts of the LO signal and $\tilde{d}_I$ and $\tilde{d}_Q$ are the distortion terms that are uncorrelated with $s_I[n]$ and $s_Q[n]$. Furthermore, $g_{II}[n]$, $g_{IQ}[n]$, $g_{QI}[n]$ and $g_{QQ}[n]$ are linear causal filters. Based on the expressions given in (13) it would be straightforward to calculate the power of the leakages from LO port to the output port, but first g_{II}, g_{IQ}, g_{QI} and g_{QQ} filters should be specified. Considering the fact that the proposed 4D-MP model has the memory of M, it can be concluded that $g_{II}[n]$, $g_{IQ}[n]$, $g_{QI}[n]$ and $g_{QQ}[n]$ can take nonzero values only for $n = 0, 1, \cdots, M$. Then, utilizing the same approach as in (8), it can be stated that

$$R_{y_I s_I}[k] = \sum_{l=0}^{M} g_{II}[l] R_{s_I s_I}[k-l] \quad , \; k = 0, 1, \cdots, M, \tag{14a}$$

$$R_{y_I s_Q}[k] = \sum_{l=0}^{M} g_{IQ}[l] R_{s_Q s_Q}[k-l] \quad , \; k = 0, 1, \cdots, M, \tag{14b}$$

$$R_{y_Q s_I}[k] = \sum_{l=0}^{M} g_{QI}[l] R_{s_I s_I}[k-l] \quad , \; k = 0, 1, \cdots, M, \tag{14c}$$

$$R_{y_Q s_Q}[k] = \sum_{l=0}^{M} g_{QQ}[l] R_{s_Q s_Q}[k-l] \quad , \; k = 0, 1, \cdots, M. \tag{14d}$$

In equations of (14) it has been assumed that real and imaginary parts of LO signal are uncorrelated, which means that $\mathbb{E}\{s_I[n]s_Q[n-k]\} = 0$ for $k = 0, 1, \cdots, M$. Now, by applying the same approach as used in specifying filters $h_{II}[n]$ and $h_{QI}[n]$ from equations in (12), it can be declared that

$$\mathbf{g}_{II} = \mathbf{\Lambda}_{s_I}^{-1}\mathbf{R}_{y_I s_I}, \tag{15a}$$
$$\mathbf{g}_{IQ} = \mathbf{\Lambda}_{s_Q}^{-1}\mathbf{R}_{y_I s_Q}, \tag{15b}$$
$$\mathbf{g}_{QI} = \mathbf{\Lambda}_{s_I}^{-1}\mathbf{R}_{y_Q s_I}, \tag{15c}$$
$$\mathbf{g}_{QQ} = \mathbf{\Lambda}_{s_Q}^{-1}\mathbf{R}_{y_Q s_Q}, \tag{15d}$$

where $\mathbf{g}_{II}$, $\mathbf{g}_{IQ}$, $\mathbf{g}_{QI}$, $\mathbf{g}_{QQ}$, $\mathbf{R}_{y_I s_I}$, $\mathbf{R}_{y_I s_Q}$, $\mathbf{R}_{y_Q s_I}$ and $\mathbf{R}_{y_Q s_Q}$ are $(M+1)\times 1$ vectors defined as follows

$$\mathbf{g}_{II} = [g_{II}[0] \quad g_{II}[1] \quad \cdots \quad g_{II}[M]]^T, \tag{16a}$$
$$\mathbf{g}_{IQ} = [g_{IQ}[0] \quad g_{IQ}[1] \quad \cdots \quad g_{IQ}[M]]^T, \tag{16b}$$
$$\mathbf{g}_{QI} = [g_{QI}[0] \quad g_{QI}[1] \quad \cdots \quad g_{QI}[M]]^T, \tag{16c}$$
$$\mathbf{g}_{QQ} = [g_{QQ}[0] \quad g_{QQ}[1] \quad \cdots \quad g_{QQ}[M]]^T, \tag{16d}$$

$$\mathbf{R}_{y_I s_I} = [R_{y_I s_I}[0] \quad R_{y_I s_I}[1] \quad \cdots \quad R_{y_I s_I}[M]]^T, \tag{16e}$$
$$\mathbf{R}_{y_I s_Q} = [R_{y_I s_Q}[0] \quad R_{y_I s_Q}[1] \quad \cdots \quad R_{y_I s_Q}[M]]^T, \tag{16f}$$
$$\mathbf{R}_{y_Q s_I} = [R_{y_Q s_I}[0] \quad R_{y_Q s_I}[1] \quad \cdots \quad R_{y_Q s_I}[M]]^T, \tag{16g}$$
$$\mathbf{R}_{y_Q s_Q} = [R_{y_Q s_Q}[0] \quad R_{y_Q s_Q}[1] \quad \cdots \quad R_{y_Q s_Q}[M]]^T, \tag{16h}$$

and $\mathbf{\Lambda}_{s_I}$ and $\mathbf{\Lambda}_{s_Q}$ are $(M+1)\times(M+1)$ matrices whose elements are $\Lambda_{s_I}(i,j) = R_{s_I s_I}[i-j]$ and $\Lambda_{s_Q}(i,j) = R_{s_Q s_Q}[i-j]$, respectively, for $i = 1, 2, \cdots, (M+1)$ and $j = 1, 2, \cdots, (M+1)$. After calculating $\mathbf{g}_{II}$, $\mathbf{g}_{IQ}$, $\mathbf{g}_{QI}$ and $\mathbf{g}_{QQ}$ filters in (15), it would be possible to represent the equations in (13) in the frequency domain as

$$Y_I(f) = G_{II}(f)S_I(f) + G_{IQ}(f)S_Q(f) + \tilde{D}_I(f), \tag{17a}$$
$$Y_Q(f) = G_{QI}(f)S_I(f) + G_{QQ}(f)S_Q(f) + \tilde{D}_Q(f), \tag{17b}$$

where $G_{II}(f)$, $G_{IQ}(f)$, $G_{QI}(f)$ and $G_{QQ}(f)$ are the Fourier transforms of $g_{II}[n]$, $g_{IQ}[n]$, $g_{QI}[n]$ and $g_{QQ}[n]$ filters, respectively. Since the LO signal is ideally a single tone signal at the carrier frequency, its baseband equivalent is also a single tone at $f = 0$, which means that in equations in (17) the terms $S_I(f)$ and $S_Q(f)$ are zero at $f \neq 0$. Therefore, equations in (17) can be simplified as

$$Y_I(f) = G_{II}(0)S_I(f) + G_{IQ}(0)S_Q(f) + \tilde{D}_I(f), \tag{18a}$$
$$Y_Q(f) = G_{QI}(0)S_I(f) + G_{QQ}(0)S_Q(f) + \tilde{D}_Q(f), \tag{18b}$$

where $G_{II}(0)$, $G_{IQ}(0)$, $G_{QI}(0)$ and $G_{QQ}(0)$ can be defined as follows

$$G_{II}(0) = G_{II}(f)\Big|_{f=0} = \sum_{k=0}^{M} g_{II}[k], \tag{19a}$$
$$G_{IQ}(0) = G_{IQ}(f)\Big|_{f=0} = \sum_{k=0}^{M} g_{IQ}[k], \tag{19b}$$
$$G_{QI}(0) = G_{QI}(f)\Big|_{f=0} = \sum_{k=0}^{M} g_{QI}[k], \tag{19c}$$
$$G_{QQ}(0) = G_{QQ}(f)\Big|_{f=0} = \sum_{k=0}^{M} g_{QQ}[k]. \tag{19d}$$

TABLE II
MEASURED AND ESTIMATED VALUES OF CARRIER FEED-THROUGH.

Measured carrier feed-through	Estimated carrier feed-through
-53.92 dBm	-54.28 dBm

Finally, by expressing the equations in (17) in time domain, it can be stated that,

$$y_I[n] = G_{II}(0)s_I[n] + G_{IQ}(0)s_Q[n] + \tilde{d}_I[n], \tag{20a}$$
$$y_Q[n] = G_{QI}(0)s_I[n] + G_{QQ}(0)s_Q[n] + \tilde{d}_Q[n]. \tag{20b}$$

Consequently, the amount of power of the LO term that is leaked into the I output is $G_{II}^2(0)P_{s_I} + G_{IQ}^2(0)P_{s_Q}$, and the power of the LO term that is leaked into the Q output is $G_{QI}^2(0)P_{s_I} + G_{QQ}^2(0)P_{s_Q}$, where P_{s_I} and P_{s_Q} are the power of $s_I[n]$ and $s_Q[n]$, respectively.

The values of measured and estimated carrier feed-through are reported in Table II. The measured carrier feed-through in Table II is obtained by passing an all zero input data signal through the measured I/Q modulator in Figure 2, whereas the estimated carrier feed-through is calculated based on the expressions given in (20).

C. Third Order Intermodulation Intercept Point (IIP3)

IIP3 is a parameter for describing the non-linear behavior of any non-linear device. In practice, IIP3 can be defined as the ratio between the power of the desired linear term to the power of 3rd order intermodulation term (IM3) [5], [28].

Based on [27], for measuring IIP3 of an I/Q modulator the Q input port needs to be terminated first and then a two-tone waveform, which is called $x_t[n]$, is loaded to the I input port. By doing this, all the terms that depend on Q input are removed in the memory polynomial expression of the outputs in (1) and (2) as follows

$$y_I[n] = \sum_{m=0}^{M_I}\sum_{p_1=0}^{P_{x,I}^r}\sum_{p_3=0}^{P_{s,I}^r}\sum_{p_4=0}^{P_{s,I}^i} a\,(m,p_1,0,p_3,p_4)\times \Big(x_t^{p_1}[n-m]s_I^{p_3}[n-m]s_Q^{p_4}[n-m]\Big), \tag{21a}$$

$$y_Q[n] = \sum_{m=0}^{M_Q}\sum_{p_1=0}^{P_{x,Q}^r}\sum_{p_3=0}^{P_{s,Q}^r}\sum_{p_4=0}^{P_{s,Q}^i} b\,(m,p_1,0,p_3,p_4)\times \Big(x_t^{p_1}[n-m]s_I^{p_3}[n-m]s_Q^{p_4}[n-m]\Big). \tag{21b}$$

The basis functions in (21) that depend on the real or imaginary parts of LO signal (the basis functions with $p_3 > 0$ or $p_4 > 0$) have a very small portion of the total power in $y_I[n]$ and $y_Q[n]$. For instance, based on the 4D-Mp model trained based on the measurement setup in Figure 2, less than 0.01 percent of the power in $y_I[n]$ and $y_Q[n]$ comes from the terms that depend on the LO signal when the Q input is terminated. Therefore, for estimating the IIP3 it is more

reasonable to neglect the terms that depend on LO signal in (21), and simplify the expressions for $y_I[n]$ and $y_Q[n]$ as

$$y_I[n] \approx \sum_{m=0}^{M_I} \sum_{p_1=0}^{P^r_{x,I}} a\left(m, p_1, 0, 0, 0\right) x_t^{p_1}[n-m], \tag{22a}$$

$$y_Q[n] \approx \sum_{m=0}^{M_Q} \sum_{p_1=0}^{P^r_{x,Q}} b\left(m, p_1, 0, 0, 0\right) x_t^{p_1}[n-m]. \tag{22b}$$

Moreover, $x_t[n]$ in (21) and (22) is a two-tone signal defined as follows

$$x_t[n] = A\cos\left(2\pi f_1 n\right) + A\cos\left(2\pi f_2 n\right), \tag{23}$$

where f_1 and f_2 should be chosen close enough so that the 3rd order inter-modulation (IM3) terms, located at frequencies $(2f_1 - f_2)$ and $(2f_2 - f_1)$, are inside the desired output frequency band. For measuring the IIP3, it would be enough to extract the linear term and the IM3 term from the baseband equivalent of the output signal, by applying suitable filters [5]. However, due to the memory effect, different tones and different IM3 terms would have different powers. It can be shown that the exponential term resulted from the first tone, located at frequency f_1, and the exponential term resulted from the first IM3 term, located at frequency $(2f_1 - f_2)$, are as follows

$$\begin{aligned} T_{\text{Low}} =& e^{j2\pi f_1 n}\Bigg(\frac{A}{2}\sum_{m=0}^{M}(a_{m1000} + jb_{m1000})e^{-j2\pi f_1 m} \\ &+ \frac{9A^3}{8}\sum_{m=0}^{M}(a_{m3000} + jb_{m3000})e^{-j2\pi f_1 m}\Bigg), \end{aligned} \tag{24a}$$

$$\begin{aligned} \text{IM3}_{\text{Low}} =& e^{j2\pi(2f_1-f_2)n}\times \\ &\left(\frac{3A^3}{8}\sum_{m=0}^{M}(a_{m3000} + jb_{m3000})e^{-j2\pi(2f_1-f_2)m}\right). \end{aligned} \tag{24b}$$

In equations of (24), the terms T_{Low} and IM3_{Low} refer to the lower tone, located at frequency f_1, and the lower IM3 component, located at frequency $(2f_1 - f_2)$, in the spectrum of $y[n] = y_I[n] + jy_Q[n]$ (since without loss of generality it has been assumed that $f_1 < f_2$). Next, in order to measure IIP3, it is more common to first assume a small value for A to make sure that the I/Q modulator is working in the linear region, then by changing the value of A it will be possible to find 2 lines for the power variations of T_{Low} and IM3_{Low} in dB versus the value of A [5]. For small values of A the term that depends on A^3 in (24a) is negligible, compared with the term that depends on A, so it will be enough to consider only the linear part of (24a) for calculating IIP3. Finally, according to the fact that these 2 lines will have different slopes, the value of IIP3 will be equal to the value of A at the intercept point of the 2 lines [5]. So, in the case of the proposed 4D-MP model for mixers, it is enough to find A in equations in (24) in a way that the linear part of T_{Low} and the IM3_{Low} term have the same power. Therefore, the IIP3 is equal to

$$\text{IIP3}_{\text{Low}} = \left|\frac{4\sum_{m=0}^{M}\gamma_{m1}e^{-j2\pi f_1 m}}{3\sum_{m=0}^{M}\gamma_{m3}\left[e^{-j2\pi(2f_1-f_2)m}\right]}\right|^{\frac{1}{2}}, \tag{25}$$

where $\gamma_{m1} = a_{m1000} + jb_{m1000}$ and $\gamma_{m3} = a_{m3000} + jb_{m3000}$ are defined for simplicity in notation. With following the same procedure, it will be possible to compute higher IIP3 based on the linear term from the higher tone, located at frequency f_2, and the higher IM3 term, located at frequency $(2f_2 - f_1)$, as follows

$$\begin{aligned} T_{\text{High}} =& e^{j2\pi f_2 n}\Bigg(\frac{A}{2}\sum_{m=0}^{M}\gamma_{m1}e^{-j2\pi f_2 m} \\ &+ \frac{9A^3}{8}\sum_{m=0}^{M}\gamma_{m3}e^{-j2\pi f_2 m}\Bigg), \end{aligned} \tag{26a}$$

$$\text{IM3}_{\text{High}} = e^{j2\pi(2f_2-f_1)n}\left(\frac{3A^3}{8}\sum_{m=0}^{M}\gamma_{m3}e^{-j2\pi(2f_2-f_1)m}\right), \tag{26b}$$

$$\text{IIP3}_{\text{High}} = \left|\frac{4\sum_{m=0}^{M}\gamma_{m1}e^{-j2\pi f_2 m}}{3\sum_{m=0}^{M}\gamma_{m3}\left[e^{-j2\pi(2f_2-f_1)m}\right]}\right|^{\frac{1}{2}}. \tag{26c}$$

It is obvious that in general the two IIP3 values defined in (25) and (26c) are not equal, which is a result of the presence of memory effects in the I/Q modulator. In other words, for a memoryless I/Q modulator, M should be replaced by 0 in (25) and (26c), which will result in $\text{IIP3}_{\text{Low}} = \text{IIP3}_{\text{High}} = \sqrt{\frac{4\gamma_{01}}{3\gamma_{03}}}$.

The values of measured IIP3 over the measurement setup, illustrated in Figure 2, and the estimated IIP3 based on the 4D-MP model are reported in Table III. In order to measure the lower IIP3 and the upper IIP3 in Table III, a real two-tone input signal, with tones located at frequencies $f_1 = 3.5$ MHz and $f_2 = 4.5$ MHz, is applied to the I input port of the I/Q modulator. Then by measuring the baseband equivalent of the RF output signal and extracting its components at frequencies f_1 and f_2, and also by extracting the lower intermodulation term at frequency $2f_1 - f_2 = 2.5$ MHz and the upper intermodulation term at frequency $2f_2 - f_1 = 5.5$ MHz, it would be possible to compute the lower and the upper IIP3 terms. As it can be seen in Table III, the estimated value of IIP3 follows its measured value for both upper and lower IIP3 values. Moreover, as was expected, there is a small

TABLE III
MEASURED AND ESTIMATED VALUES OF THE LOWER IIP3 AND THE HIGHER IIP3.

Measured lower IIP3	Estimated lower IIP3	Measured higher IIP3	Estimated higher IIP3
12.42 dBm	12.39 dBm	12.36 dBm	12.33 dBm

difference between the values of upper IIP3 and lower IIP3, where the lower IIP3 is a bit larger than the upper IIP3.

D. Quadrature Phase Error and I/Q Amplitude Balance

These parameters are defined to measure the amount of leaked signals from the I branch to the Q branch and vice versa. These parameters' effects are mainly recognized as I/Q imbalance (IQI). In a memory-less I/Q imbalanced system, the output signal, $y[n]$, can be expressed based on the input signal, $x[n]$, as [29]

$$y[n] = \alpha x[n] + \beta x^*[n] + w[n]. \tag{27}$$

In (27), α and β are IQI coefficients and $w[n]$ is the additive noise term.

In an ideal scenario where there are no leakages between the in-phase and quadrature branches, the in-phase output and quadrature output exhibit balanced amplitudes and no phase mismatch. However, the presence of leakages between these branches introduces an amplitude mismatch and phase mismatch between the in-phase and quadrature outputs. In literature, the term "I/Q amplitude balance" is commonly used to describe the amplitude mismatch, while "quadrature phase error" refers to the phase mismatch. If the quadrature phase error is equal to θ and the I/Q amplitude balance is a, then based on the discussion in [30] it can be stated that

$$y_I^{\text{RF}}[n] = \gamma x_I[n] \cos\left(2\pi f_{\text{LO}} n + \phi_{\text{LO}}\right), \tag{28a}$$
$$y_Q^{\text{RF}}[n] = a\,\gamma x_Q[n] \sin\left(2\pi f_{\text{LO}} n + \phi_{\text{LO}} + \theta\right). \tag{28b}$$

In equations of (28), $y_I^{\text{RF}}[n]$ and $y_Q^{\text{RF}}[n]$ are the in-phase and the quadrature RF outputs, respectively, γ is the total gain of the in-phase branch, and ϕ_{LO} is the initial phase of the LO signal. It can be proved that the following relationship holds between (α, β) and (a, θ) [31],

$$\alpha = \frac{1 + ae^{j\theta}}{2} \qquad , \qquad \beta = \frac{1 - ae^{j\theta}}{2}. \tag{29}$$

However, based on the proposed 4D-MP model and Bussgang analysis for memory polynomials, the input-output relationship of an I/Q modulator can be expressed as in (4), which will result in

$$y[n] = h[n] * x[n] + \tilde{h}[n] * x^*[n] + d[n], \tag{30}$$

where $y[n] = y_I[n] + jy_Q[n]$, $x[n] = x_I[n] + jx_Q[n]$ and

$$h[n] = \frac{h_{II}[n] + h_{QQ}[n]}{2} + j\left(\frac{h_{QI}[n] - h_{IQ}[n]}{2}\right), \tag{31a}$$
$$\tilde{h}[n] = \frac{h_{II}[n] - h_{QQ}[n]}{2} + j\left(\frac{h_{QI}[n] + h_{IQ}[n]}{2}\right). \tag{31b}$$

The terms $h_{II}[n]$ and $h_{QI}[n]$ can be computed based on equations given in (12), likewise $h_{IQ}[n]$ and $h_{QQ}[n]$ can be computed as follows

$$\mathbf{h}_{IQ} = \mathbf{\Lambda}_{x_Q}^{-1}\mathbf{R}_{y_I x_Q}, \tag{32a}$$
$$\mathbf{h}_{QQ} = \mathbf{\Lambda}_{x_Q}^{-1}\mathbf{R}_{y_Q x_Q}, \tag{32b}$$

where

$$\mathbf{h}_{IQ} = [h_{IQ}[0] \quad h_{IQ}[1] \quad \cdots \quad h_{IQ}[M]]^T, \tag{33a}$$
$$\mathbf{h}_{QQ} = [h_{QQ}[0] \quad h_{QQ}[1] \quad \cdots \quad h_{QQ}[M]]^T, \tag{33b}$$
$$\mathbf{R}_{y_I x_Q} = [R_{y_I x_Q}[0] \quad R_{y_I x_Q}[1] \quad \cdots \quad R_{y_I x_Q}[M]]^T, \tag{33c}$$
$$\mathbf{R}_{y_Q x_Q} = [R_{y_Q x_Q}[0] \quad R_{y_Q x_Q}[1] \quad \cdots \quad R_{y_Q x_Q}[M]]^T, \tag{33d}$$

and $\mathbf{\Lambda}_{x_Q}$ is an $(M+1) \times (M+1)$ matrix, whose elements are $\Lambda_{x_Q}(i,j) = R_{x_Q x_Q}[i-j]$ for $i = 1, 2, \cdots, M+1$ and $j = 1, 2, \cdots, M+1$. Therefore, since there are memory effects in the modeled I/Q modulator, it will not be possible to express its input-output relationship in the form of (27), which means that it is not possible to define a single pair of parameters as quadrature phase error and I/Q amplitude balance based on the developed 4D-MP model. However, according to the input-output relationship given in (30), if $x[n]$ be a single tone complex signal centered at frequency f_0, then equation (30) can be simplified as

$$y[n] = H(f_0)x[n] + \tilde{H}(-f_0)x^*[n] + d[n], \tag{34}$$

where $H(f_0)$ and $\tilde{H}(f_0)$ are Fourier transforms of $h[n]$ and $\tilde{h}[n]$, respectively, computed at frequency $f = f_0$,

$$H(f_0) = \sum_{n=0}^{M} h[n]e^{-j2\pi f_0 n}, \tag{35a}$$
$$\tilde{H}(-f_0) = \sum_{n=0}^{M} \tilde{h}[n]e^{j2\pi f_0 n}. \tag{35b}$$

Now since the input-output relationship given in (34) is in the form of (27), it would be possible to compute quadrature phase error and I/Q amplitude balance as follows

$$\Big[\text{Quadrature Phase Error at } f_0\Big] = \measuredangle\Big(H(f_0) - \tilde{H}(-f_0)\Big) \triangleq \Theta(f_0), \tag{36a}$$

$$\Big[\text{I/Q Amplitude Balance at } f_0\Big] = \Big|H(f_0) - \tilde{H}(-f_0)\Big| \triangleq A(f_0). \tag{36b}$$

Consequently, quadrature phase error and I/Q amplitude balance parameters will depend on the frequency at which the input signal is located, so they should be considered as frequency-dependent parameters, instead of fixed parameters as introduced for memory-less systems in (29). Accordingly, quadrature phase error and I/Q amplitude balance can be defined as frequency-dependant functions represented by $\Theta(f)$ and $A(f)$, respectively. The defined $\Theta(f)$ and $A(f)$ in (36), should be computed in the whole frequency band of the I/Q modulator data input signal. The predicted I/Q amplitude balance and quadrature phase error for the I/Q modulator under test are given in Figures 6 and 7, respectively, where similar to Figure 5 the solid black lines represent the estimated I/Q amplitude balance expressed in (36b) and the estimated quadrature phase error in (36a), the dotted red lines represent the measured I/Q amplitude balance and quadrature phase error over the measurement setup illustrated in Figure 2, and the dashed blue lines represent the measured I/Q amplitude

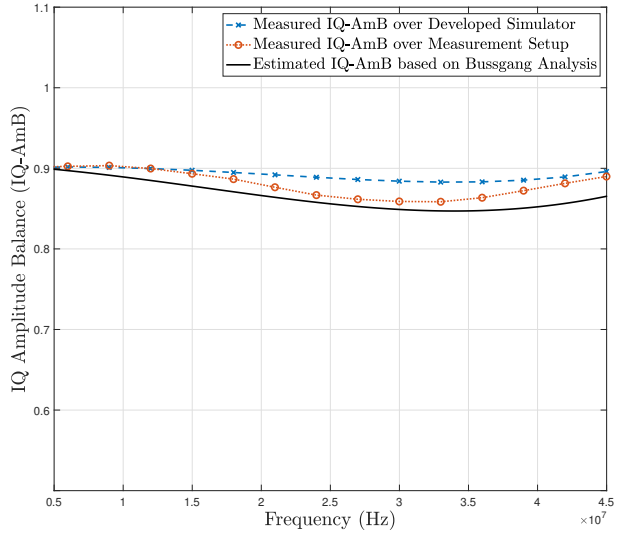

Fig. 6. Predicted and measured I/Q amplitude balance over the measured frequency band.

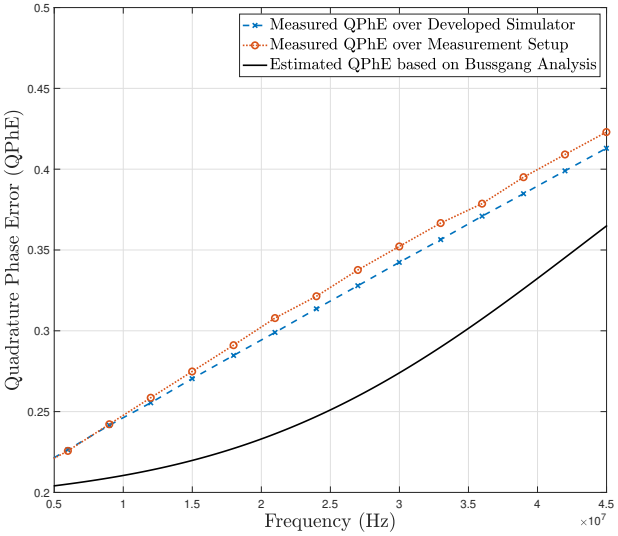

Fig. 7. Predicted and measured quadrature phase error in radians over the measured frequency band.

balance and quadrature phase error over an I/Q modulator simulator which is developed based on the 4D-MP model expressed in (1) and (2). It should be noted that in order to measure the I/Q amplitude balance and the quadrature phase error (over the measurement setup or the simulator) at a specific frequency, f_0, a complex valued single tone input signal, $x(n) = e^{j2\pi f_0 n}$, is applied to the input ports of the I/Q modulator. However, for predicting the I/Q amplitude balance and the quadrature phase error in the desired frequency band based on the Bussgang analysis, a wideband QAM modulated signal has been employed as the input signal to the I/Q modulator, to estimate $h[n]$ and $\tilde{h}[n]$ filters.

As illustrated in Figure 6, the measured I/Q amplitude balance over the developed I/Q modulator simulator follows the I/Q amplitude balance measured over the laboratory setup given in Figure 2, however, there are some small differences between the two measured values of I/Q amplitude balance (less than 3 percent). Furthermore, a small gap exists between the Bussgang-based predicted I/Q amplitude balance, as expressed in (36b), and the measured I/Q amplitude balance, where the gap is less than 2 percent of the measured I/Q amplitude balance. This discrepancy primarily stems from the distinct structures of the input signals employed. In the case of calculating the predicted I/Q amplitude balance, a wideband signal is utilized, resulting in in-band distortion within the I/Q modulator due to the presence of higher-order nonlinearities within the mixers. Conversely, the measured I/Q amplitude balance is obtained using a single-tone input signal, which lacks any in-band distortions.

It is obvious from Figure 7 that the measured quadrature phase error over the developed I/Q modulator simulator follows the quadrature phase error measured through the laboratory measurement setup. In addition, as depicted in Figure 7, there is a gap between the predicted quadrature phase error based on Bussgang analysis, expressed in (36a), and the measured quadrature phase error, where the gap is less than 0.1 radian. Similar to the case of I/Q amplitude balance, the primary factor contributing to this gap is the distinct structure of the input signals utilized for deriving the measured and the estimated quadrature phase error.

Hence, the experimental validation demonstrates that the marginal discrepancy observed in the I/Q amplitude balance plots in Figure 6 and the disparity in the quadrature phase error plots in Figure 7 are predominantly attributed to the introduction of additional in-band distortion when utilizing a wideband input signal, in contrast to the employment of a single tone input signal. Consequently, one can conclude that the predicted I/Q amplitude balance and quadrature phase error, as expressed in (36), offer improved estimations of the performance of a practical communication link, as they account for the influence of existing in-band distortion.

V. Conclusion

This study introduces a novel 4D-MP-based algorithm to effectively model the non-ideal behavior of mixers within the context of I/Q modulators. The proposed 4D-MP model incorporates a memory polynomial algorithm, enabling the inclusion of both linear and non-linear leakages between the in-phase and quadrature branches of an I/Q modulator. The experimental measurement results obtained from the developed measurement setup confirm the high precision of the proposed 4D-MP model in predicting the non-ideal behavior of both mixers and I/Q modulators. The model successfully captures the intricate characteristics and performance deviations with a remarkable level of accuracy. The 4D-MP model can also extract the key parameters associated with I/Q modulators such as conversion gain, carrier feed-through, IIP3, quadrature phase error, and I/Q amplitude balance. Derivation of these parameters offers valuable insights into the behavior and performance of I/Q modulators. Additionally, the 4D-MP model

serves as a highly reliable simulator for mixers, making it suitable for design and measurement purposes. In future work, the proposed 4D-MP model can be further employed to design a digital pre-distortion unit to compensate for the non-ideal behaviors of mixers and I/Q modulators at the transmitter side of a communication link. This would contribute to enhancing overall system performance and mitigating signal distortions.

ACKNOWLEDGMENT

This research has been carried out in Gigahertz-ChaseOn Bridge Center in a project financed by Chalmers, Ericsson, Gotmic, Infineon, Kongsberg, Saab, and UniqueSec.

REFERENCES

[1] S. A. Maas, *Nonlinear microwave and RF circuits*, 2nd ed. Norwood, MA, USA: Artech House, 2003.

[2] B. Zhang, L. Tong, B. Gao, B. Yang, S. Li, S. Liang, and F. Nian, "A study on the memory effect of mixer," in *IEEE Radar Conf.*, Florence, Italy, 2020.

[3] M. Valkama, A. Springer, and G. Hueber, "Digital signal processing for reducing the effects of RF imperfections in radio devices—an overview," in *Proc. of 2010 IEEE Int. Symp. on Circuits and Syst.*, Paris, France, 2010, pp. 813–816.

[4] M. Othmani, N. Boulejfen, A. Brihuega, F. M. Ghannouchi, M. Allén, and M. Valkama, "Delta-sigma modulator-embedded digital predistortion for 5G transmitter linearization," *IEEE Trans. Commun.*, vol. 70, no. 8, pp. 5558–5571, 2022.

[5] B. Razavi, *RF microelectronics*, 2nd ed. Upper Saddle River, NJ, USA: Prentice Hall, 2012.

[6] D. F. Williams, F. Ndagijimana, K. A. Remley, J. A. Dunsmore, and S. Hubert, "Scattering-parameter models and representations for microwave mixers," *IEEE Trans. Microw. Theory Tech.*, vol. 53, no. 1, pp. 314–321, 2005.

[7] A. Ozgun, T. Nesimoglu, and S. Demir, "A multi-box behavioural mixer model and its validation using measurements," in *IEEE MTT-S Int. Microw. Symp. (IMS)*, Boston, MA, USA, 2019, pp. 607–610.

[8] A. Cidronali, "Broad-band poly-harmonic wiener modeling of mixers based on large-signal vector measurements," in *IEEE MTT-S Int. Microw. Symp. (IMS)*, San Francisco, CA, USA, 2016.

[9] K. Vandermot, W. Van Moer, J. Schoukens, and Y. Rolain, "Understanding the nonlinearity of a mixer using multisine excitations," in *2006 IEEE Instrum. and Meas. Technol. Conf. Proc.*, 2006, pp. 1205–1209.

[10] L. Anttila, M. Valkama, and M. Renfors, "Frequency-selective I/Q mismatch calibration of wideband direct-conversion transmitters," *IEEE Trans. on Circuits and Syst. II: Express Briefs*, vol. 55, no. 4, pp. 359–363, 2008.

[11] M. Valkama, "Advanced I/Q signal processing for wideband receivers models and algorithms," Ph.D. dissertation, Tampere University of Technology, 2001.

[12] H. Cao, A. S. Tehrani, C. Fager, T. Eriksson, and H. Zirath, "I/Q imbalance compensation using a nonlinear modeling approach," *IEEE Trans. Microw. Theory Tech.*, vol. 57, no. 3, pp. 513–518, 2009.

[13] S. Yamada, O. Boric-Lubecke, and V. M. Lubecke, "Cancellation techniques for LO leakage and DC offset in direct conversion systems," in *2008 IEEE MTT-S Int. Microw. Symp. Digest*, 2008, pp. 1191–1194.

[14] B. S. Sengar and A. Kumar, Amitesh, "Mixer design," in *RF Circuits For 5G Applications: Designing with mmWave Circuitry*. Hoboken, NJ, USA: Wiley Online Library, 2023, ch. 6, pp. 107–122.

[15] J. Tuthill and A. Cantoni, "Efficient compensation for frequency-dependent errors in analog reconstruction filters used in IQ modulators," *IEEE Trans. Commun.*, vol. 53, no. 3, pp. 489–496, 2005.

[16] M. Mansour, A. Zekry, M. K. Ali, and H. Shawkey, "Integrated multi-band RF transceiver design for multi-standard applications using 130 nm CMOS technology," *Microelectronics J.*, vol. 110, p. 105006, 2021.

[17] Y. Gao, A. Wen, W. Zhang, W. Jiang, J. Ge, and Y. Fan, "Ultra-wideband photonic microwave I/Q mixer for zero-IF receiver," *IEEE Trans. Microw. Theory Tech.*, vol. 65, no. 11, pp. 4513–4525, 2017.

[18] L. Anttila, M. Valkama, and M. Renfors, "Circularity-based I/Q imbalance compensation in wideband direct-conversion receivers," *IEEE Trans. Veh. Technol.*, vol. 57, no. 4, pp. 2099–2113, 2008.

[19] O. Tanovic, A. Megretski, Y. Li, V. Stojanovic, and M. Osqui, "Equivalent baseband models and corresponding digital predistortion for compensating dynamic passband nonlinearities in phase-amplitude modulation-demodulation schemes," *IEEE Trans. Signal Process.*, vol. 66, no. 22, pp. 5972–5987, 2018.

[20] C. Cheng, Z. Peng, W. Zhang, and G. Meng, "Volterra-series-based nonlinear system modeling and its engineering applications: A state-of-the-art review," *Mech. Syst. and Signal Process.*, vol. 87, pp. 340–364, 2017.

[21] L. Ding, G. T. Zhou, D. R. Morgan, Z. Ma, J. S. Kenney, J. Kim, and C. R. Giardina, "A robust digital baseband predistorter constructed using memory polynomials," *IEEE Trans. Commun.*, vol. 52, no. 1, pp. 159–165, 2004.

[22] N. Hajiabdolrahim, S. Wang, C. Fager, H. V. Hünerli, and T. Eriksson, "A real-valued 4D memory polynomial algorithm for mixer modeling," in *51-st Eur. Microw. Conf.*, London, UK, 2022.

[23] D. R. Morgan, Z. Ma, J. Kim, M. G. Zierdt, and J. Pastalan, "A generalized memory polynomial model for digital predistortion of RF power amplifiers," *IEEE Trans. Signal Process.*, vol. 54, no. 10, pp. 3852–3860, 2006.

[24] N. Y. Ermolova and O. Tirkkonen, "Theoretical characterization of memory polynomial models with gaussian inputs," *IEEE Signal Process. Lett.*, vol. 16, no. 8, pp. 651–654, 2009.

[25] O. T. Demir and E. Björnson, "The Bussgang decomposition of nonlinear systems: Basic theory and MIMO extensions [lecture notes]," *IEEE Signal Process. Mag.*, vol. 38, no. 1, pp. 131–136, 2020.

[26] M. Bashar, H. Q. Ngo, K. Cumanan, A. G. Burr, P. Xiao, E. Björnson, and E. G. Larsson, "Uplink spectral and energy efficiency of cell-free massive MIMO with optimal uniform quantization," *IEEE Trans. Commun.*, vol. 69, no. 1, pp. 223–245, 2020.

[27] "Baseband Response Characterization of I-Q Modulators," Tektronix, Tech. Rep. 37W-29553-1, Feb. 2014. [Online]. Available: https://download.tek.com/document/37W_29553_1_MR_Letter.pdf

[28] F. Belveze and P. Baudin, "Specifying receiver IP2 and IP3 based on tolerance to modulated blockers," *IEEE Trans. Commun.*, vol. 56, no. 10, pp. 1677–1682, 2008.

[29] A. E. Canbilen, S. S. Ikki, E. Basar, S. S. Gultekin, and I. Develi, "Impact of I/Q imbalance on amplify-and-forward relaying: Optimal detector design and error performance," *IEEE Trans. Commun.*, vol. 67, no. 5, pp. 3154–3166, 2019.

[30] T. C. Schenk, E. Fledderus, and P. F. Smulders, "Performance analysis of zero-IF MIMO OFDM transceivers with IQ imbalance," *J. Commun.*, vol. 2, no. 7, pp. 9–19, 2007.

[31] N. Kolomvakis, M. Matthaiou, and M. Coldrey, "IQ imbalance in multiuser systems: Channel estimation and compensation," *IEEE Trans. Commun.*, vol. 64, no. 7, pp. 3039–3051, 2016.